Improvement of adherence and anticorrosion properties of an epoxy-polyamide coating on steel by incorporation of an indole-3 butyric acid-modified nanomagnetite

Anh Truc Trinh, Thu Trang Nguyen, Thu Thuy Thai, Thi Xuan Hang To, Xuan Hoan Nguyen, Anh Son Nguyen, Maëlenn Aufray, Nadine Pébère

Abstract In this study, synthesized magnetite (Fe_3O_4) nanoparticles were treated with a corrosion inhibitor, indole-3 butyric acid (IBA) and incorporated in an epoxy-polyamide coating. The coating was applied on a carbon steel substrate. For comparison, coatings without particles or with nontreated Fe_3O_4 particles were also prepared. The IBA-modified nanomagnetite (IBA–Fe_3O_4) was characterized by infrared spectroscopy and Zeta potential measurements. The inhibitive action of IBA was shown by electrochemical measurements (polarization curves) performed for a bare carbon steel in 0.1 M NaCl solution containing Fe_3O_4 or IBA–Fe_3O_4 nanoparticles. Adherence and anticorrosion properties of the epoxy-based coatings containing Fe_3O_4 or IBA–Fe_3O_4 were compared to those of the pure epoxy-polyamide resin by dry and wet adherence measurements and by salt spray test. The results showed significant improvement of the film adherence and higher corrosion protection of the carbon steel in the presence of IBA–Fe_3O_4. It was concluded that the IBA effect was restricted to the metal/coating interface.

Keywords Fe_3O_4 nanoparticles, Epoxy-polyamide-based coating, Corrosion inhibitor, Carbon steel, Adherence tests, Salt spray test

A. T. Trinh (✉), T. T. Nguyen, T. T. Thai, T. X. H. To (✉)
Laboratory for Protective Coatings, Institute for Tropical Technology, VAST, 18, Hoang Quoc Viet, Hanoi, Vietnam
e-mail: anhtruc.trinh@itt.vast.vn

T. X. H. To
e-mail: ttxhang@itt.vast.vn

X. H. Nguyen
Faculty of Chemistry, VNU University of Science, 19, Le Thanh Tong, Hanoi, Vietnam

A. S. Nguyen, M. Aufray, N. Pébère
Université de Toulouse, CIRIMAT, UPS/INPT/CNRS, 4, allée Emile Monso, CS 44362, 31030 Toulouse Cedex 4, France

Introduction

Recently, the introduction of nanoparticles in protective coatings has attracted numerous investigations. The most commonly used nanoparticles are SiO_2, TiO_2, ZnO, Al_2O_3, Fe_2O_3, and clays.[1–10] For corrosion protection of metals, the addition of nanoparticles in organic coatings offers an acceptable environmental solution. The major documented benefit of the incorporation of nanoparticles in polymer coatings is reinforcement of barrier effect and improvement of mechanical properties. These effects are due to their tiny size and large specific surface area. The dispersion of nanoparticles induces additional interactions with the organic matrix and thus enhances the barrier properties. In addition, good dispersion of lamellar or plate-like shaped charges (e.g., clay platelets) in coatings increases the length of the diffusion paths of corrosive species through the film and thus improves the barrier effect.[6,11] The presence of nanoparticles can also reinforce the coating resistance against hydrolytic degradation and increase the coating adherence.[10,11] Iron oxide pigments are commonly used in organic coatings to protect ferrous substrates, particularly structural steels, due to their nontoxic, weather-resistant, and mainly opaque properties.[12–19] Magnetite iron oxide pigments (Fe_3O_4) are known as black pigments and used for a wide range of applications. They confer high anticorrosion efficiency in various binders.[13] Although the protective mechanism is not yet well established, it has been proposed that incor-

poration of magnetite in paints leads to interactions between the paint and the steel, delaying the corrosion process.[14] It has been also suggested that the magnetite pigments create an alkaline environment at the metal/coating interface which limits the corrosion process.[16–18] Moreover, the interactions between the magnetite pigments and carboxyl groups in alkyd (or polyester modified by fatty acid) binders can lead to metal soaps formation which can act as inhibitors at the metal/organic coating interface.[16,19] However, iron oxide pigments agglomerate easily due to their small size and high surface energy. This phenomenon affects their efficiency when they are directly incorporated in an organic matrix. To improve the dispersion, a modification of the surface of the nanoparticle is required. Recently, the magnetite nanoparticles were encapsulated by organic or polymeric compounds and used as corrosion inhibitors for carbon steel in acidic medium.[20–22] Their efficiencies were significant in 1 M HCl solution.

In continuation of our quest for developing corrosion inhibitors with high efficiency, the present work aims to prepare treated magnetite nanoparticles and then to incorporate them in an epoxy-based coating. In previous works, indole-3 butyric acid (IBA) was attached to montmorillonite clay (MMT) which is an inert filler.[23,24] It is well known that the main role of MMT within polymer matrixes is to improve their barrier effect. Resulting from this modification, the IBA-modified clay improved the corrosion performance of epoxy coatings by both an increase of the barrier properties of the film and by the inhibitive action of the IBA molecules at the carbon steel/coating interface.[23,24] In the present work, IBA was used with an active filler, the nanomagnetite. IBA-modified nanomagnetite was used as an additive in an epoxy-polyamide coating to enhance the corrosion protection, particularly the coating adherence on the steel surface. As a matter of fact, a high level of adherence is required between the paint and the metal to prevent delamination. Nanomagnetite was prepared by hydrothermal method and modified by the IBA molecules (IBA–Fe_3O_4). A salt spray test was conducted to evaluate the corrosion protection of the epoxy-based coatings containing or not the nanoparticles. Adherence of the coatings on carbon steel surface was measured by three-point bending and was also evaluated by cross-cut test after different immersion times in an aqueous solution.

Experimental

Materials

For the nanoparticles synthesis, $FeCl_3{\cdot}6H_2O$, $FeSO_4{\cdot}7H_2O$, and KOH were purchased from Merck. Indole-3 butyric acid (IBA), purchased from Sigma Aldrich, was used as received.

The epoxy resin was unmodified diglycidyl ether of bisphenol A, Epotec YD 011-X75. Epoxy equivalent weight was about 460–490 g eq^{-1}. The hardener was a polyamide 307D-60; equivalent weight per active H was 266 g eq^{-1}. Both compounds were purchased from Kukdo Chemical Co., Ltd. (Korea).

Carbon steel plates (150 mm × 100 mm × 2 mm) were used as substrates. The chemical composition of the steel in weight percent was C = 0.35, Mn = 0.65, Si = 0.25, P = 0.035, and Fe to balance. The sample surface was abraded with successive SiC papers from 80 to 600 grades and washed with ethanol. The magnetite (Fe_3O_4) and IBA-modified magnetite (IBA–Fe_3O_4) nanoparticles were incorporated at a concentration of 3 wt% in the pre-polymer mixture with xylene as solvent. This content, optimized by preliminary tests, was sufficient to achieve the required properties. The pre-polymer mixtures (with or without particles) were applied by spin-coating at a speed of 600 rpm for 90 s. After polymerization and drying at room temperature for 24 h, the coatings were about 30 μm thick (measured by Minitest 600 Erichen digital meter).

Synthesis and surface modification of the Fe_3O_4 nanoparticles

The magnetite (Fe_3O_4) nanoparticles were prepared following the protocol previously used[25] and is briefly recalled here: a mixture of $FeCl_3{\cdot}6H_2O/FeSO_4{\cdot}7H_2O$ (molar ratio Fe^{2+}/Fe^{3+} = 1/1) was dissolved with distilled water. Under stirring, a KOH solution was added to the solution until the formation of a precipitate occurred. The resulting slurry mixture was transferred to a Teflon-lined stainless steel autoclave. Hydrothermal reaction was conducted at 150°C for 7 h. After reaction, the precipitate was washed with distilled water to remove impurity ions (Cl^-, SO_4^{2-}, K^+) and dried in a vacuum oven at 80°C for 12 h.

IBA (0.2 g) was dissolved in a 50 mL water/ethanol mixture (1/19 ratio). Then, the Fe_3O_4 nanoparticles (1 g) were dispersed by an IKA T10 Ultra-Turrax disperser (30,000 rpm for 10 min) and then mechanically stirred for 180 min. The precipitate was filtered and washed with ethanol several times to remove the excess IBA. The IBA–Fe_3O_4 nanoparticles were finally dried in a vacuum oven at 60°C for 24 h. The synthesized Fe_3O_4 nanoparticles were previously characterized by X-ray diffraction.[25] All peaks on the XRD patterns properly correspond with the Fe_3O_4 standard (symmetry *Fd*-3*m*, *a* = 8.378 Å, cubic crystal structure). Similar XRD patterns were obtained for IBA–Fe_3O_4.

Analytical characterizations

Fourier transform infrared spectra were recorded with a Nexus 670 Nicolet spectrometer equipped with

DTGS KBr detector. Each spectrum was scanned 32 times at a resolution of 4 cm^{-1} in the 400–4000 cm^{-1} region. The transmission spectra were recorded using KBr pellets.

The amount of remaining IBA in the water/ethanol mixture was determined by UV–Vis spectroscopy at λ_{max} = 224 nm using GBC Cintra 40 spectrometer, from a calibration curve obtained for a series of standard solutions (from 1×10^{-3} to 3×10^{-2} mol L^{-1} of IBA):

$$A = 138.8C + 0.0026,$$

where C is the concentration of IBA (in mol L^{-1}) and A is the absorption intensity at 224 nm.

The IBA loading on the Fe_3O_4 particles was calculated from the remaining IBA content in the water/ethanol mixture and was about 0.03 g (0.17 g of remaining IBA from 0.2 g of the initial IBA mixture with 1 g of Fe_3O_4). Thus, the IBA loading was 3 wt% (15% of the initial IBA were fixed on the Fe_3O_4 nanoparticles).

The IBA release from the IBA–Fe_3O_4 nanoparticles at different pH values (3, 7, and 10) was also determined using the following protocol: 0.05 g of IBA–Fe_3O_4 was stirred with distilled water (25 mL) for 24 h. Then, the solution was filtered and the IBA content was determined by UV–Vis spectroscopy at 224 nm. Release experiments were performed in triplicate.

Field-emission scanning electron microscope (FE-SEM) observations were carried out to examine the surface morphology of the magnetite/epoxy polymer composite (using a Jeol JSM 7800F). The microphotographs were recorded at an accelerating voltage of 5.0 kV at different magnifications.

The surface charge of the nanoparticles was determined at 25°C by Zeta potential measurements using a Zetameter Phoremeter IV. The particles were dispersed in distilled water with 5 mmol L^{-1} of KCl in an ultrasonic bath before being injected in the Zeta cell. The Schmoluchowski equation was employed to calculate the Zeta potential values.[25]

Electrochemical measurements

The polarization curves were obtained with a classical three-electrode cell in which the bare carbon steel electrode served as the working electrode with an exposed area of 1 cm^2. A saturated calomel electrode and a large platinum sheet were used as reference and counter electrodes, respectively. The electrochemical cell was open to air and was kept at room temperature. The corrosive medium was a 0.1 M NaCl solution. The polarization curves for the carbon steel in the solution containing IBA (10^{-3} M) or Fe_3O_4 (3 wt%) or IBA–Fe_3O_4 (3 wt%) were recorded after 2 h of immersion in the electrolyte, at a scan rate of 1 mV s^{-1}, starting from −0.9 to −0.1 V SCE^{-1}. Two trials were performed to ensure reproducibility.

Differential scanning calorimetry (DSC)

DSC experiments were carried out with a Mettler DSC 1 Star System apparatus to determine the glass transition temperature (T_g) of the coatings. Aluminum pans containing about 10 mg of paints were heated three times from 0 to 160°C at a heating rate of 10°C min^{-1} under a continuous flow of nitrogen. The T_g was determined as $T_{g\infty}$ (after post-curing) by the onset point with a ±1°C sensitivity.

Salt spray test

Salt spray test was used in order to evaluate the corrosion protection of the samples. The test was performed according to ASTM B117 using a Q-FOGCCT-600 chamber. Scribes were made on the samples before exposure to the salt spray. The specimens were placed inside the salt spray chamber at an angle of 20° without any contact with each other or with any metallic material. A solution of 5% NaCl was sprayed on the samples. The spraying was maintained for the duration of the test. The temperature of the chamber was kept as 35°C. The samples were evaluated according to ASTM D1654 after 240 h of exposure.

Adherence tests

The crosscut adherence test was performed according to ASTM D 3359 method B to evaluate the adherence of the coatings during aging in distilled water. The adherence was measured using crosshatch cutter six blades with 1 mm spaces between cutting edges. An adhesive test tape with adhesive strength of 9.5 N per 25 mm (ISO 2409) was immediately applied to the cross-cut coating surface. The tape was removed by a quick pull and the coating removal content was determined. The test was also performed after different immersion times in distilled water. The coatings were dried by clean tissue paper to remove the surface water and placed at room temperature for 10 min to be sure of surface dryness. The adhesive strength was evaluated by using the following expression:

$$\text{Adhesive loss}\,(\%) = \frac{x}{25}100,$$

where x is the number of squares of detached coating and 25 is the total number of squares on the intact coating.

To measure the adherence more accurately, the three-point bending test was carried out according to ISO 14679-1997. Before testing, coated steel plates were carefully sawn into samples of size 50 mm × 10 mm.

The samples were degreased with ethanol and ultrasonicated in an ethanol bath for 10 min. Then, they were placed in a silicone mold between two clamping plates. The assembly was closed and a 5 mL stoichiometric epoxy-amine ratio polymer mixture (Dow Chemical, Midland, MI, USA—DGEBA DER^{TM} 332 and DETA from Aldrich, St. Louis, MO, USA, respectively) was injected into the mold. 25 mm × 5 mm × 4 mm stiffener epoxy blocks were made according to the ISO 14679-1997 Standard, and as described in previous work.[26] Stiffener block polymerization was carried out at ambient temperature (23 ± 2°C) for 24 h. Then, the assembly was sequentially placed in a dry oven at 60°C for 3 h and at 120°C for 1 h. An Instron 3367 tensile testing machine (Norwood, MA, USA) was used with a 5000 N full-scale load cell with a sensitivity of ±0.5% of the measured values, and a crosshead displacement speed of 0.5 mm min^{-1} (±0.5%). Bluehill software (Instron) controlled the apparatus parameters. The ultimate load (F_{max} measured on the load–displacement curve) was taken as the adherence parameter. For each tested sample, the failure must be verified as an adhesive failure and not as a cohesive one. Good average values and low standard errors of F_{max} were achieved and validated by testing eight samples for each system.

Results and discussion

First, FTIR spectroscopy and Zeta potential measurements were presented to show the presence of the IBA molecules on the nanomagnetite surface. Then, the inhibitive effect of IBA on the corrosion of the carbon steel was characterized by polarization curves. Afterward, the IBA content on the treated Fe_3O_4 and the release of IBA from the IBA–Fe_3O_4 nanoparticles determined by UV–Vis spectroscopy were presented. Finally, the protection of the carbon steel was discussed from the salt spray test and from the adherence measurements by the three-point bending (before aging) and the cross-cut test (before and after aging).

Characterization of the IBA–Fe_3O_4 nanoparticles

Figure 1 presents the FTIR spectra of pure IBA, Fe_3O_4, and IBA–Fe_3O_4 nanoparticles. The characteristic bands of the spectra are given in Table 1. The spectrum of the Fe_3O_4 shows bands at 578 and 454 cm^{-1}.[27,28] These bands were also found in the spectrum of IBA–Fe_3O_4. The hydrocarbon chain of the IBA molecule gave bands at 2946, 2853 cm^{-1} and IBA–Fe_3O_4 presented similar bands at 2920, 2852 cm^{-1}. The C=O and C-O–H characteristic peaks were observed at 1694 and 1427 cm^{-1} for the IBA molecule.[29] In the IBA–Fe_3O_4 spectrum, these peaks are shifted to 1629 and 1385 cm^{-1}. The comparison of the three spectra (Fig. 1) shows the presence of the IBA molecules on the surface of the Fe_3O_4 nanoparticles.

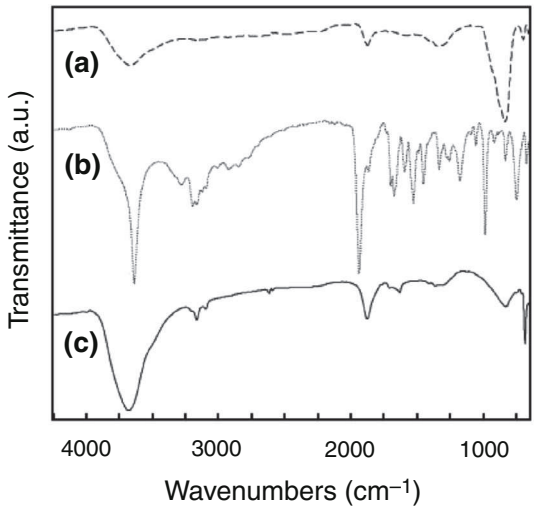

Fig. 1: FTIR spectra of: (a) Fe_3O_4, (b) IBA, and (c) IBA–Fe_3O_4

Table 1: Characteristic bands of FTIR spectra obtained for IBA, Fe_3O_4 and IBA–Fe_3O_4

IBA (cm^{-1})	Fe_3O_4 (cm^{-1})	IBA–Fe_3O_4 (cm^{-1})	Bond
–	578	579	Fe–O
	454	434	
2946, 2853	–	2920, 2852	$-CH_2$
1694		1629	–C = O
1427		1385	–C–O–H

Figure 2 shows the surface charge distribution for Fe_3O_4 and IBA–Fe_3O_4 nanoparticles. The Fe_3O_4 nanoparticles have an average surface charge value of about −20 mV. The negative charge on the particles surface can be attributed to the adsorption of hydroxyl group from the alkaline medium during the hydrothermal reaction. For the IBA–Fe_3O_4 nanoparticles, the average surface charge was shifted to a more negative region, about −50 mV. The increase in the negative charge of the IBA–Fe_3O_4 confirmed the presence of the IBA molecules on the nanoparticles.

The polarization curves obtained for the carbon steel in the 0.1 M NaCl solutions containing Fe_3O_4 or IBA–Fe_3O_4 nanoparticles are presented in Fig. 3. The curves without nanoparticles (blank solution) and with IBA at 10^{-3} M are also reported for comparison. In the presence of ''free'' IBA in the solution, it can be seen that the corrosion potential is shifted in the anodic direction (about 100 mV) and the anodic current densities are significantly lower by comparison with the blank solution, particularly near the corrosion potential. This result confirmed the inhibitive properties of IBA[23,24] and showed that the compound is an anodic inhibitor. The polarization curves obtained in

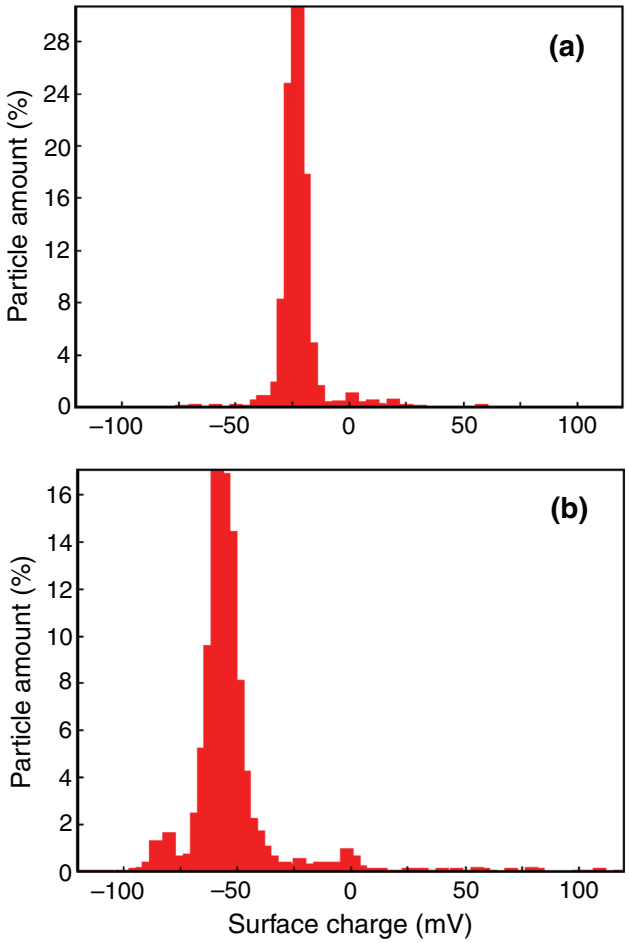

Fig. 2: Surface charge distribution on: (a) Fe_3O_4 and (b) IBA–Fe_3O_4 nanoparticles

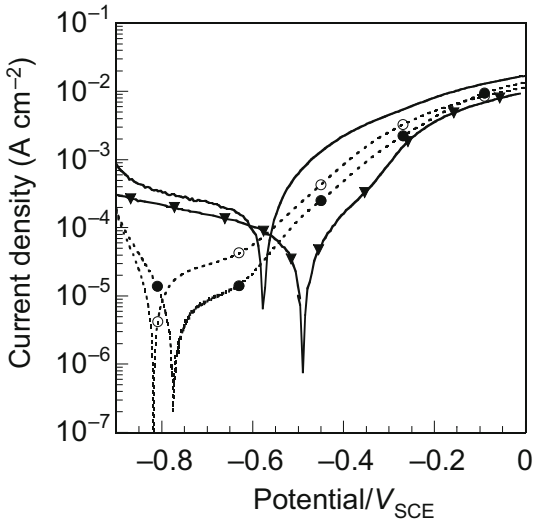

Fig. 3: Polarization curves obtained for the carbon steel electrode after 2 h of immersion in the 0.1 M NaCl solution: (○) 3 wt% of Fe_3O_4, (●) 3 wt% of IBA–Fe_3O_4, (▼) 10^{-3}M IBA and (——) blank solution (pH 6)

the presence of Fe_3O_4 or IBA–Fe_3O_4 presented similar shape. The corrosion potential is shifted toward cathodic potentials by comparison with the blank solution and the current densities are significantly lower. For both types of magnetite, accumulation of particles on the carbon steel surface was observed after the electrochemical measurements. This observation can explain the results observed in the presence of the nanoparticles. However, for the solution containing the IBA–Fe_3O_4, the corrosion potential is shifted toward anodic values and the anodic current densities are lower, similar to the curve obtained in the presence of "free" IBA. The electrochemical results showed the inhibitive effect of the IBA on the corrosion of the carbon steel and confirmed that the IBA molecules are attached on the Fe_3O_4 nanoparticles.

Characterization of the epoxy-polyamide coatings

The glass transition temperatures, T_g, of the epoxy-polyamide coatings with or without nanoparticles were determined by DSC. The values are reported in Table 2. A slight decrease of the T_g values is observed for the coatings containing the Fe_3O_4 and the IBA–Fe_3O_4 nanoparticles.

Numerous investigations have examined the effect of nanoparticles addition on the glass transition temperature. On the one hand, the incorporation of nanoparticles (such as nanoclay or iron oxide) in a polyepoxy matrix often increases its T_g, due to an additional crosslinking which decreases the polymer mobility.[23] On the other hand, the addition of nanoparticles might decrease the T_g value due to the decrease of the crosslinking density and/or interphase formation.[30–32] In order to verify these hypotheses, fracture surface of the epoxy-polyamide coatings containing Fe_3O_4 or IBA–Fe_3O_4 were observed by FE-SEM and presented in Fig. 4. Nanoparticles have grain size of about 50 nm. For both coatings, particles agglomeration can be observed. In the presence of IBA–Fe_3O_4, some fragments of polymer remained attached to the fillers (Fig. 4d) and this feature was not observed in the presence of Fe_3O_4 (Figs. 4a and 4b). This result revealed higher adherence between the polymer and the fillers and thus indicated a better compatibility between the epoxy-polyamide matrix and the IBA–Fe_3O_4 surface which can explain the decrease of T_g.

Table 2: T_g values for the different coatings

	Pure epoxy-polyamide coating	Epoxy-polyamide coating containing Fe_3O_4	Epoxy-polyamide coating containing IBA–Fe_3O_4
$T_{g/onset}$ (°C)	71	68	65

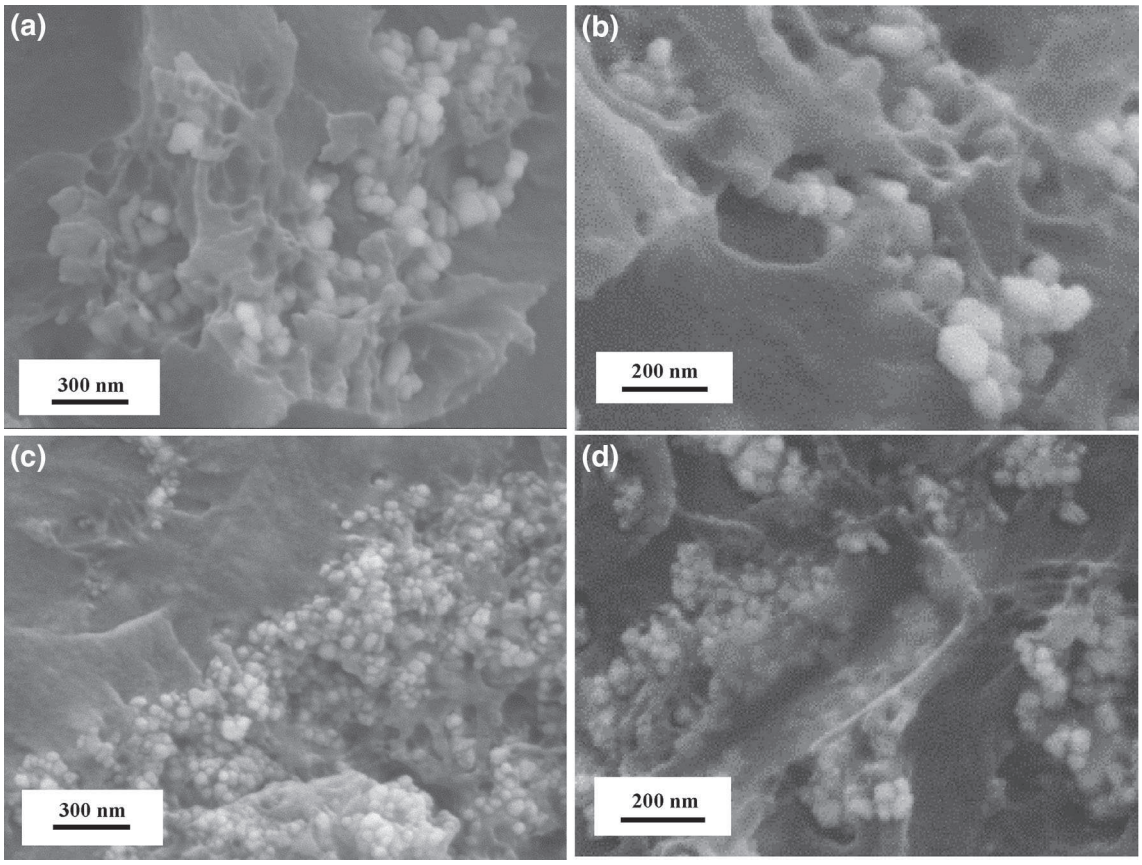

Fig. 4: FE-SEM micrographs of a fracture surface for the epoxy-polyamide coatings containing: (a, b) Fe_3O_4 and (c, d) IBA–Fe_3O_4

Corrosion protection performance

Electrochemical impedance measurements were first performed to characterize the barrier properties of the coatings. The results are not presented here because the impedance diagrams were similar for the coatings containing the two types of nanoparticles indicating that there was no influence of the magnetite treatment by IBA on the impedance response. Nonetheless, the impedance results showed that the addition of treated or nontreated magnetite in the epoxy-polyamide coatings allowed the barrier properties to remain high during exposure to a 0.5 M sodium chloride solution while those of pure epoxy-polyamide resin continually decreased during immersion. This result underlined that the incorporation of Fe_3O_4 or IBA–Fe_3O_4 improved the coating performance. Since the impedance results did not allow the IBA influence to be shown, salt spray test in the presence of a scratch was conducted as an accelerated corrosion test to evaluate the corrosion resistance of the carbon steel covered with the epoxy-polyamide coating containing or not the nanoparticles (Fe_3O_4 and IBA–Fe_3O_4). Pictures of the samples after 240 h exposure to the salt spray are shown in Fig. 5 and the evaluation of the corrosion behavior, according to ASTM D1654, is presented in Table 3. Numerous blisters associated with corrosion products are observed on the edge of the scratch for the pure epoxy-polyamide coating. This behavior corresponds to a loss of adherence of the coating.[33] Brown corrosion products are visible inside the scratch. Development of blisters and corrosion products are limited for the epoxy-polyamide coating containing Fe_3O_4 and a few corrosion products in the scratch and few blisters around the scratch are observed for the sample with IBA–Fe_3O_4. The rust creepage from the scribe for the pure epoxy system was higher than for the epoxy containing the nanoparticles (Table 3). According to the ASTM D1654, the rating number is 7 for the pure epoxy coating and 8 for the epoxy containing Fe_3O_4 or IBA–Fe_3O_4 (after 240 h of exposure to the salt spray). The salt spray results indicated that the presence of Fe_3O_4 or IBA–Fe_3O_4 improved the corrosion protection of the carbon steel.

To show the IBA effect on the corrosion protection, the release of IBA in distilled water, from the IBA–Fe_3O_4 particles was measured by UV–Vis spectroscopy for three pH values (Fig. 6). It is observed in Fig. 6 that the IBA release increases for the high pH value. It can be recalled that the corrosion process induces an increase of the local pH due to the cathodic reaction of oxygen reduction. Thus, the release of IBA, favored in

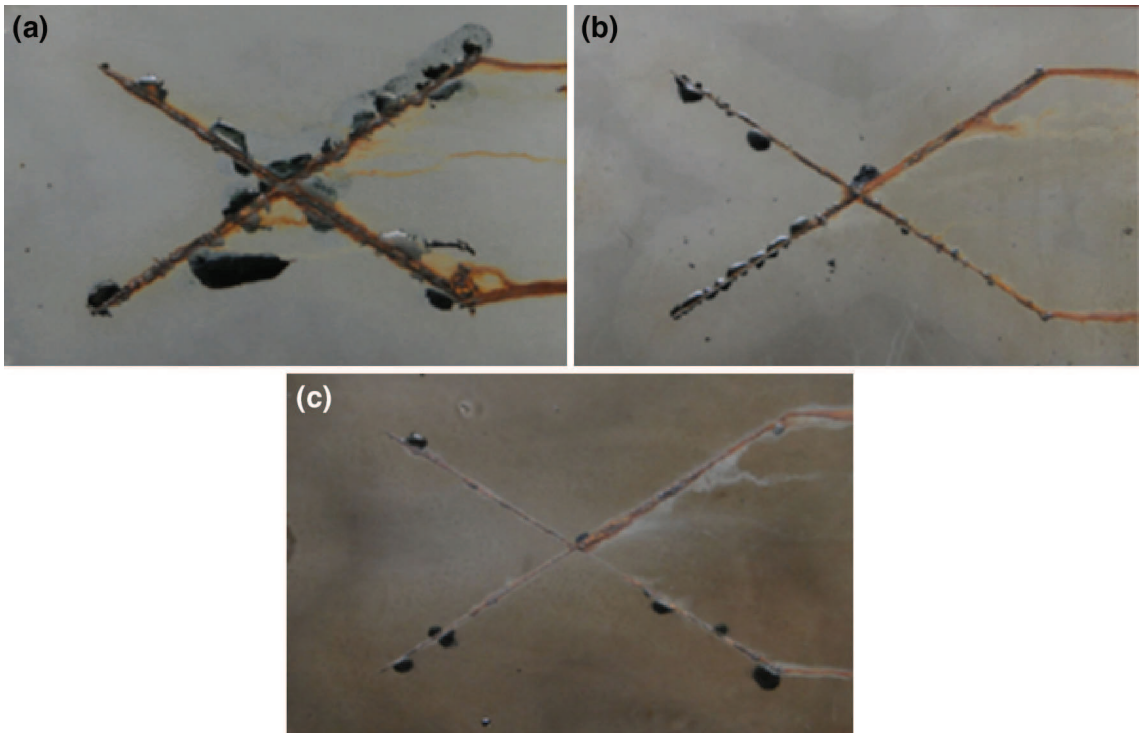

Fig. 5: Salt spray test results obtained after 240 h for the carbon steel coated with the epoxy-polyamide film: (a) without nanoparticles, (b) with Fe_3O_4 and (c) with IBA–Fe_3O_4

Table 3: Salt spray test results after 240 h exposure according to ASTM D1654 standard

Samples	Creepage from scribe	
	Rust creepage (mm)	Rating number
Epoxy-polyamide coating	1.27	7
Epoxy-polyamide coating containing Fe_3O_4	0.79	8
Epoxy-polyamide coating containing IBA–Fe_3O_4	0.64	8

alkaline conditions, will lead to the corrosion inhibition of the carbon steel.

Adherence measurements

To characterize the effect of the Fe_3O_4 particles on the behavior of the steel/coating interface, two adherence tests were performed. First, the cross-cut adherence test was performed to evaluate the influence of water penetration at the steel/coating interface during aging in distilled water. According to Funke,[34,35] the adherence under wet conditions is more meaningful for corrosion protection than dry adherence (initial adherence before aging). Many coatings showed excellent tensile adherence to metal but lost the adherence after exposure to pure water at room or elevated temperatures. A thin film of water at the interface is apparently responsible for the loss of adherence. Images of the coatings surface before (as-prepared

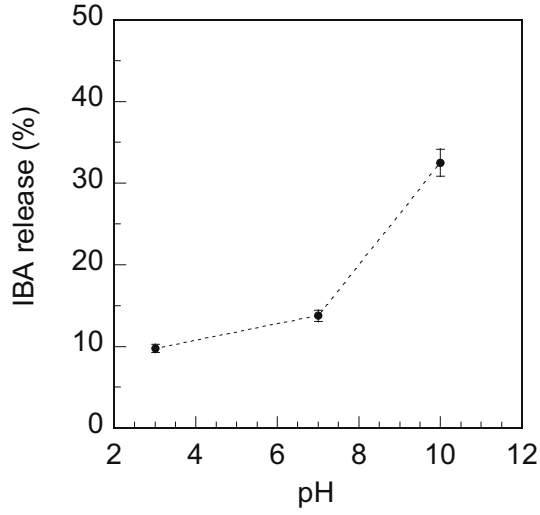

Fig. 6: Release amount of IBA from the IBA–Fe_3O_4 particles vs pH in distilled water

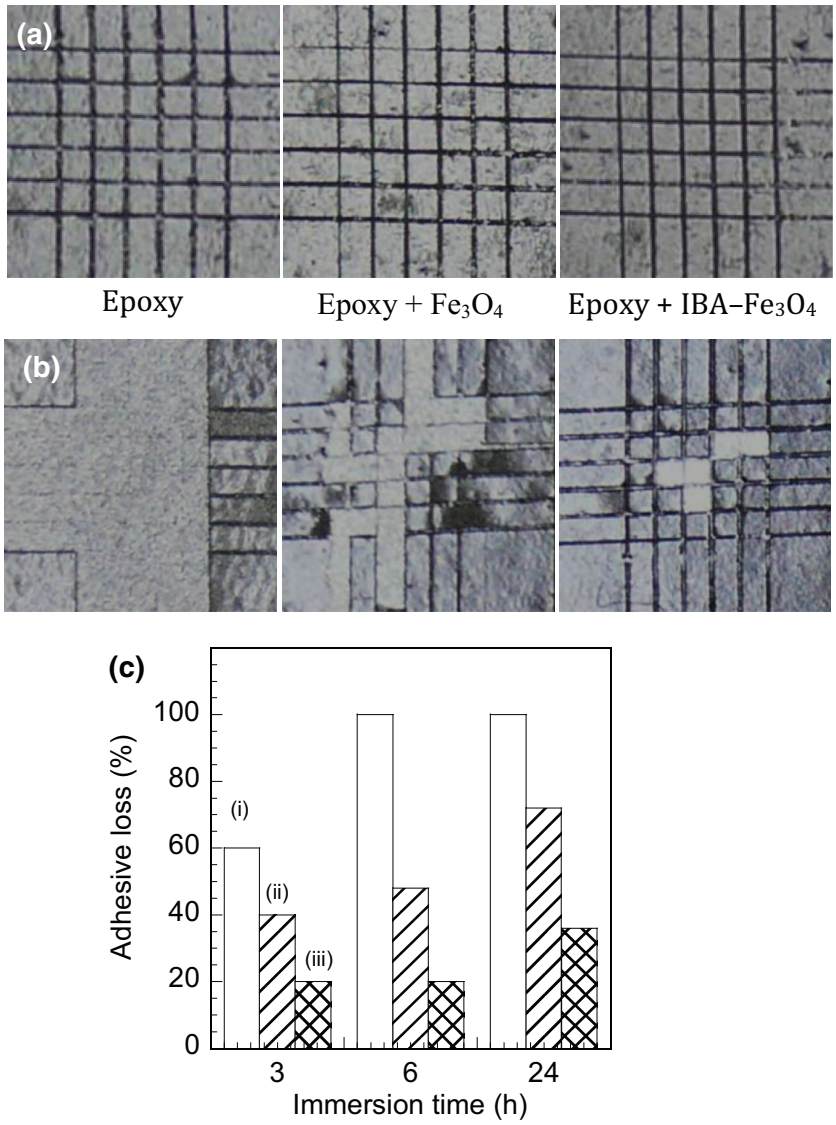

Fig. 7: (a) and (b) Images of the samples surface after the crosscut test: (a) dry adhesion and (b) wet adhesion after 6 h of immersion in distilled water; (c) delaminated area showing the adhesive loss vs immersion time in water: (i) coating without nanoparticles, (ii) coating with Fe_3O_4, and (iii) with IBA–Fe_3O_4

samples) and after wet adherence (6 h of immersion) are shown in Figs. 7a and 7b, respectively. It can be seen that for the as-prepared samples, the crosscut area is not significantly affected by the addition of Fe_3O_4 and IBA–Fe_3O_4: there is no adhesion loss after the test for the three samples (Fig. 7a). On the contrary, after 6 h of exposure to distilled water, the film without nanoparticles is completely detached whereas only some squares of coatings are detached for the films containing Fe_3O_4 or IBA–Fe_3O_4 (Fig. 7b). The variation of the adhesive loss for the three coatings vs immersion time in distilled water is shown in Fig. 7c. It is observed that the adhesive loss of the coating without nanoparticles increases rapidly with the immersion time, while the adhesive loss of coatings containing the particles increases slowly, particularly for the coating containing IBA–Fe_3O_4. This improvement can be explained by the cooperative bonds between the Fe_3O_4 nanoparticles and the oxide layer at the steel/coating interface. For the coating containing IBA–Fe_3O_4, the wet adherence improvement can be also attributed to the IBA release in the presence of water, which reacted with iron oxides at the steel surface.[36] From the cross-cut test, it was not possible to discriminate between the adherences of the three systems at the initial state (as-prepared samples). Thus, the three-point bending test was performed to better characterize the interfacial phenomena (the failure initiation is well defined in this test) at the initial state (i.e., before aging).

Figure 8a gives, as an example, the load vs displacement recorded during the three-point bending test for

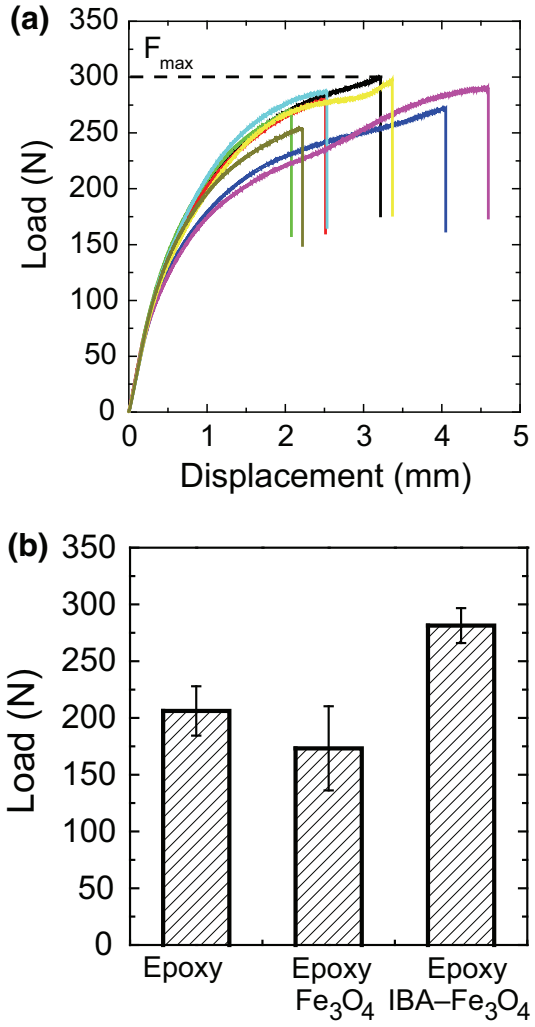

Fig. 8: (a) Load vs displacement for the steel surface covered by the epoxy-polyamide film containing IBA–Fe_3O_4 (results of eight independent trials are shown on the figure) and (b) Comparison of the adherence results obtained from the three-point bending test for the coatings: without nanoparticles, with Fe_3O_4 and with IBA–Fe_3O_4

the coating containing IBA–Fe_3O_4. The ultimate load values (F_{max}) for the three systems are compared in Fig. 8b. It is interesting to note that the coating containing IBA–Fe_3O_4 presents the highest values for the ultimate load indicating an improvement of the adherence for this coating. For the other coatings (neat epoxy-polyamide coating and epoxy-polyamide coatings containing nontreated magnetite), the measured values were similar by taking into account the reproducibility. From these results, it is possible to show a higher performance for the coating containing IBA–Fe_3O_4 before aging which cannot be observed by the crosscut test.

From the adherence measurements coupled with the salt spray test, an improvement in both the adherence (dry and wet conditions) and the corrosion protection when the IBA–Fe_3O_4 particles were incorporated in the coatings was seen. Thus, it can be concluded that the main action of IBA–Fe_3O_4 is limited at the metal/coating interface.

Discussion

In aqueous solutions, IBA showed a significant inhibition effect. It is known that the inhibitive action of organic compounds containing S, N, and O is due to the formation of a covalent type bond between the metal and the lone pair of electrons in the molecule.[37] The chemisorption of IBA on the steel surface can take place between the π-electrons and the iron vacant *d*-orbital. More particularly, this adsorption can take place at the metal/coating interface when the IBA molecules are released from the Fe_3O_4 particles due to the presence of water which penetrated through the coating. Moreover, it was shown that the IBA release (from the IBA–Fe_3O_4) was higher when the pH increases. Thus, in neutral and alkaline media, the IBA release could impede the corrosion process and confer self-healing properties to the coating. The salt spray test confirmed the beneficial effect of IBA on the corrosion protection of the carbon steel.

On the other hand, the improvement of the interactions between the coating and the metal surface was shown for the epoxy-polyamide coating containing IBA–Fe_3O_4 by the three-point bending test for the as-prepared samples. The adherence increase could be linked to the polymer network, as indicated by the decrease of T_g with the addition of Fe_3O_4 (treated or nontreated by IBA). Previous works have shown that metal oxides are able to react with the monomers, leading to a competition with the polymerization reaction.[38] The decrease of T_g could be also linked to the decrease of crosslinking density with interphase formation all around the particles (Fig. 4), which can be attributed to an incomplete curing of the composites in the presence of the nanoparticles. The unreacted functional groups might have interactions with the metal/coating interface, reinforcing the adherence of the coating on the metallic substrate.[39] It could be also mentioned that the Fe_3O_4 nanoparticles are magnetic and might migrate to the metallic surface during the curing process, changing the adherence behavior (in our case, increasing the adherence). The cross-cut tests in wet conditions clearly showed the role of the IBA–Fe_3O_4 nanoparticles at the metal/coating interface. Finally, it can be concluded that the corrosion protection was controlled by the adherence of the coatings and the action of IBA–Fe_3O_4 at the metal/coating interface was confirmed.

Conclusions

The corrosion protection of the carbon steel by epoxy-polyamide-based coatings containing Fe_3O_4 and IBA–

Fe_3O_4 nanoparticles (3 wt%) was evaluated by the salt spray test and adherence tests. It was shown that the coatings were highly protective in the presence of IBA–Fe_3O_4 nanoparticles. The inhibitive action of IBA (anodic inhibitor) on the corrosion of the carbon steel was confirmed by the polarization curves, in agreement with previous results. In the scratch (salt spray test), its inhibitive action was observed due to the release of IBA from IBA–Fe_3O_4 particles. However, the IBA content in the Fe_3O_4 is relatively low. For the long-term protection of the carbon steel, a higher content of IBA on the Fe_3O_4 particles is required. The IBA–Fe_3O_4 played a role at the coating/steel interface by strengthening the adherence before and after aging (i.e., dry and wet adherence tests). This work demonstrates that the combination of accelerated corrosion tests and adherence tests provides relevant and complementary information for a better assessment of the corrosion protection by organic coatings.

Acknowledgments This work was carried out with financial support from National Foundation for Science and Technology Development of Vietnam (NAFOSTED, Project 104.01-2011.01), Vietnamese Academy of Science and Technology (VAST, Project VAST.HTQT.Phap.02/13-14), Vietnamese National University of Hanoi (Project QG.12.05), and from CNRS, France (LIA-FOCOMAT Project).

References

1. Dhoke, SK, Khanna, AS, "Electrochemical Behavior of Nano-iron Oxide Modified Alkyd Based Waterborne Coatings." *Mater. Chem. Phys.*, **117** 550–556 (2009)
2. Ramezanzadeh, B, Attar, MM, Farzam, M, "A Study on the Anticorrosion Performance of the Epoxy-Polyamide Nanocomposites Containing ZnO Nanoparticles." *Prog. Org. Coat.*, **72** 410–422 (2011)
3. Scrinzi, E, Rossia, S, Kamarchik, P, Deflorian, F, "Evaluation of Durability of Nano-silica Containing Clear Coats for Automotive Applications." *Prog. Org. Coat.*, **71** 384–390 (2011)
4. Li, XW, Song, RG, Jiang, Y, Wang, C, Jiang, D, "Surface Modification of TiO_2 Nanoparticles and Its Effect on the Properties of Fluoropolymer/TiO_2 Nanocomposite Coatings." *Appl. Surf. Sci.*, **276** 761–768 (2013)
5. Sow, C, Riedl, B, Blanchet, P, "UV-Waterborne Polyurethane-Acrylate Nanocomposite Coatings Containing Alumina and Silica Nanoparticles for Wood: Mechanical, Optical, and Thermal Properties Assessment." *J. Coat. Technol. Res.*, **8** 211–221 (2011)
6. Huttunen-Saarivirta, E, Vaganov, GV, Yudin, VE, Vuorinen, J, "Characterization and Corrosion Protection Properties of Epoxy Powder Coatings Containing Nanoclays." *Prog. Org. Coat.*, **76** 757–767 (2013)
7. Dhoke, SK, Mangal Sinha, TJ, Khanna, AS, "Effect of Nano-Al_2O_3 Particles on the Corrosion Behavior of Alkyd Based Waterborne Coatings." *J. Coat. Technol. Res.*, **6** 353–368 (2009)
8. Dhoke, SK, Khanna, AS, "Effect of Nano-Fe_2O_3 Particles on the Corrosion Behavior of Alkyd Based Waterborne Coatings." *Corros. Sci.*, **51** 6–20 (2009)
9. Palimi, MJ, Rostami, M, Mahdavian, M, Ramezanzadeh, B, "A Study on the Corrosion Inhibition Properties of Silane-Modified Fe_2O_3 Nanoparticle on Mild Steel and Its Effect on the Anticorrosion Properties of the Polyurethane Coating." *J. Coat. Technol. Res.*, **12** 277–292 (2015)
10. Ramezanzadeh, B, Attar, MM, "Studying the Corrosion Resistance and Hydrolytic Degradation of an Epoxy Coating Containing ZnO Nanoparticles." *Mater. Chem. Phys.*, **130** 1208–1219 (2011)
11. Heidariana, M, Shishesaz, MR, Kassiriha, SM, Nematollahi, M, "Characterization of Structure and Corrosion Resistivity of Polyurethane/Organoclay Nanocomposite Coatings Prepared Through an Ultrasonication Assisted Process." *Prog. Org. Coat.*, **68** 180–188 (2010)
12. Kalendová, A, Veselý, D, Kalenda, P, "Properties of Paints with Hematite Coated Muscovite and Talc Particles." *Appl. Clay Sci.*, **48** 581–588 (2010)
13. Ulbrich, M, Kalendová, A, "Properties of Organic Coatings with Nonisometric Ferrite Particles." *Phys. Proc.*, **44** 247–255 (2013)
14. Escobar, DM, Arroyave, C, Jaramillo, F, Mattos, OR, Margarit, IC, Calderón, J, "Electrochemical Assessment of Magnetite Anticorrosive Paints." *Rev. Met.*, Vol. Extr. 97–103 (2003)
15. Escobar, DM, Arroyave, C, Calderón, J, Margarit, IC, Mattos, OR, "Paintings Pigmented with Doped Magnetite: Preliminary Evaluation of Anticorrosive Properties." *Rev. Fac. Ing. Univ. Antioq.*, **41** 21–30 (2007)
16. Sekine, I, Kato, T, "Corrosion-Protective Properties of Various Ferrite Paint Films." *Ind. Eng. Chem. Prod. Res. Dev.*, **25** 7–10 (1986)
17. Kalendova, A, "Alkalising and Neutralising Effects of Anticorrosive Pigments Containing Zn, Mg, Ca, and Sr Cations." *Prog. Org. Coat.*, **38** 199–206 (2000)
18. Hao, Y, Liu, F, Han, E, "Inhibitive Behavior and Mechanism of Ferrite Inhibition Pigment in Epoxy Paints." *J. Electrochem. Soc.*, **159** C403–C410 (2012)
19. Potapova, E, Yang, X, Grahn, M, Holmgren, A, Forsmo, SPE, Fredriksson, A, Hedlund, J, "The Effect of Calcium Ions, Sodium Silicate and Surfactant on Charge and Wettability of Magnetite." *Colloids Surf. A*, **386** 79–86 (2011)
20. Atta, AM, El-Mahdy, GA, Al-Lohedan, HA, Al-Hussain, SA, "Corrosion Inhibition of Mild Steel in Acidic Medium by Magnetite Myrrh Nanocomposite." *Int. J. Electrochem. Sci.*, **9** 8446–8457 (2014)
21. El-Mahdy, GA, Atta, AM, Al-Lohedan, HA, "Synthesis and Evaluation of Poly (Sodium 2-acrylamido-2-methylpropane sulfonate-co-styrene)/Magnetite Nanoparticle Composites as Corrosion Inhibitors for Steel." *Molecules*, **19** 1713–1731 (2014)
22. Atta, AM, El-Azabawy, OE, Ismail, HS, Hegazy, MA, "Novel Dispersed Magnetite Core-Shell Nanogel Polymers as Corrosion Inhibitors for Carbon Steel in Acidic Medium." *Corros. Sci.*, **53** 1680–1689 (2011)
23. Trinh, AT, To, TXH, Vu, KO, Dantras, E, Lacabanne, C, Oquab, D, Pébère, N, "Incorporation of an Indole-3 Butyric Acid Modified Clay in Epoxy Resin for Corrosion Protection of Carbon Steel." *Surf. Coat. Technol.*, **202** 4945–4951 (2008)
24. To, TXH, Trinh, AT, Olivier, MG, Vandermiers, C, Guerit, N, Pébère, N, "Corrosion Protection Mechanisms of Carbon Steel by an Epoxy Resin Containing Indole-3 Butyric Acid Modified Clay." *Prog. Org. Coat.*, **69** 410–416 (2010)
25. Long, LQ, Hue, TTB, Hoan, NX, Cuong, LV, Thang, PD, Hoang, T, Truc, TA, "Growth Mechanism and Stability of

Magnetite Nanoparticles Synthesized by the Hydrothermal Method.'' *J. Nanosci. Nanotechnol.*, (2015). doi:10.1166/jnn.2015.11110
26. Floch, V, Doleyres, Y, Amand, S, Aufray, M, Pébère, N, Verchère, D, ''Adherence Measurements and Corrosion Resistance in Primer/Hot-Dip Galvanized Steel Systems.'' *J. Adhes.*, **89** 339–357 (2013)
27. Kahani, SA, Jafari, M, ''A New Method for Preparation of Magnetite from Iron Oxy-hydroxide or Iron Oxide and Ferrous Salt in Aqueous Solution.'' *J. Magn. Magn. Mater.*, **321** 1951–1954 (2009)
28. Cheraghipour, E, Javadpour, S, Mehdizadeh, AR, ''Citrate Capped Superparamagnetic Iron Oxide Nanoparticles Used for Hyperthermia Therapy.'' *J. Biomed. Sci. Eng.*, **5** 715–719 (2012)
29. Roonasi, P, Holmgren, A, ''A Fourier Transform Infrared (FTIR) and Thermogravimetric Analysis (TGA) Study of Oleate Adsorbed on Magnetite Nano-particle Surface.'' *Appl. Surf. Sci.*, **255** 5891–5895 (2009)
30. Zabihi, O, Hooshafza, A, Moztarzadeh, F, Payravand, H, Afshar, A, Alizadeh, R, ''Isothermal Curing Behavior and Thermo-physical Properties of Epoxy-Based Thermoset Nanocomposites Reinforced with Fe_2O_3 Nanoparticles.'' *Thermochim. Acta*, **527** 190–198 (2012)
31. Aufray, M, Roche, AA, ''Properties of the Interphase Epoxy-Amine/Metal: Influences from the Nature of the Amine and the Metal in Adhesion.'' In: Possart, W (ed.) *Current Research and Application*, pp. 89–102. Wiley, New York, 2005
32. González, M, Martín-Fabiani, I, Baselga, J, Pozuelo, J, ''Magnetic Nanocomposites Based on Hydrogenated Epoxy Resin.'' *Mater. Chem. Phys.*, **132** 618–624 (2012)
33. Rekners, U, Kalnins, M, ''Evaluation of the Protective Properties of Organic Coatings by Using Tape and Blistering Tests.'' *Prog. Org. Coat.*, **38** 35–42 (2000)
34. Funke, W, ''Thin-Layer Technology in Organic Coatings.'' *Prog. Org. Coat.*, **28** 3–7 (1996)
35. Negele, O, Funke, W, ''Internal Stress and Wet Adhesion of Organic Coating.'' *Prog. Org. Coat.*, **28** 285–289 (1996)
36. Yamabe, H, ''Stabilization of the Polymer-Metal Interface.'' *Prog. Org. Coat.*, **28** 9–15 (1996)
37. Noor, EA, ''The Inhibition of Mild Steel Corrosion in Phosphoric Acid Solutions by Some N-Heterocyclic Compounds in the Salt Form.'' *Corros. Sci.*, **47** 33–55 (2005)
38. Devasahayam, S, ''Towards Improving Wet-Adhesion in a Metal Oxide-Polymer Coating System.'' *J. Appl. Polym. Sci.*, **99** 3318–3327 (2006)
39. Puig, M, Cabedo, L, Gracenea, JJ, Jiménez-Morales, A, Gámez-Pérez, J, Suay, JJ, ''Adhesion Enhancement of Powder Coatings on Galvanised Steel by Addition of Organo-modified Silica Particles.'' *Prog. Org. Coat.*, **77** 1309–1315 (2014)